Research Article | Vol. 26, No. 10 | 14 May 2018 | OPTICS EXPRESS 12344
Optics EXPRESS

All-silicon-based nano-antennas for wavelength and polarization demultiplexing

MINGCHENG PANMAI,[1] JIN XIANG,[1] ZHIBO SUN,[1] YUANYUAN PENG,[1] HONGFENG LIU,[1] HAIYING LIU,[1] QIAOFENG DAI,[1] SHAOLONG TIE,[2] AND SHENG LAN[1,*]

[1]*Guangdong Provincial Key Laboratory of Nanophotonic Functional Materials and Devices, School of Information and Optoelectronic Science and Engineering, South China Normal University, Guangzhou 510006, China*
[2]*School of Chemistry and Environment, South China Normal University, Guangzhou 510006, China*
[*]*slan@scnu.edu.cn*

Abstract: We propose an all-silicon-based nano-antenna that functions as not only a wavelength demultiplexer but also a polarization one. The nano-antenna is composed of two silicon cuboids with the same length and height but with different widths. The asymmetric structure of the nano-antenna with respect to the electric field of the incident light induced an electric dipole component in the propagation direction of the incident light. The interference between this electric dipole and the magnetic dipole induced by the magnetic field parallel to the long side of the cuboids is exploited to manipulate the radiation direction of the nano-antenna. The radiation direction of the nano-antenna at a certain wavelength depends strongly on the phase difference between the electric and magnetic dipoles interacting coherently, offering us the opportunity to realize wavelength demultiplexing. By varying the polarization of the incident light, the interference of the magnetic dipole induced by the asymmetry of the nano-antenna and the electric dipole induced by the electric field parallel to the long side of the cuboids can also be used to realize polarization demultiplexing in a certain wavelength range. More interestingly, the interference between the dipole and quadrupole modes of the nano-antenna can be utilized to shape the radiation directivity of the nano-antenna. We demonstrate numerically that radiation with adjustable direction and high directivity can be realized in such a nano-antenna which is compatible with the current fabrication technology of silicon chips.

OCIS codes: (290.5850) Scattering, particles; (290.4020) Mie theory; (290.4210) Multiple scattering; (050.1950) Diffraction gratings.

References and links

1. L. Novotny and N. van Hulst, "Antennas for light," Nat. Photonics **5**(2), 83–90 (2011).
2. L. Cao, P. Fan, A. P. Vasudev, J. S. White, Z. Yu, W. Cai, J. A. Schuller, S. Fan, and M. L. Brongersma, "Semiconductor nanowire optical antenna solar absorbers," Nano Lett. **10**(2), 439–445 (2010).
3. J. Zhou, Z. Zhang, Y. Wu, Z. Xia, and X. Qin, "Significantly enhanced coupling to half-space irradiation using a partially capped nanowire for solar cells," Nano Energy **45**, 61–67 (2018).
4. L. Hu and G. Chen, "Analysis of optical absorption in silicon nanowire arrays for photovoltaic applications," Nano Lett. **7**(11), 3249–3252 (2007).
5. N. Liu, M. L. Tang, M. Hentschel, H. Giessen, and A. P. Alivisatos, "Nanoantenna-enhanced gas sensing in a single tailored nanofocus," Nat. Mater. **10**(8), 631–636 (2011).
6. D. Bouchet, M. Mivelle, J. Proust, B. Gallas, I. Ozerov, M. F. Garcia-Parajo, A. Gulinatti, I. Rech, Y. D. Wilde, N. Bonod, and S. Bidault, "Enhancement and inhibition of spontaneous photon emission by resonant silicon nanoantennas," Phys. Rev. Appl. **6**(6), 064016 (2016).
7. T. Shegai, P. Johansson, C. Langhammer, and M. Käll, "Directional scattering and hydrogen sensing by bimetallic pd-au nanoantennas," Nano Lett. **12**(5), 2464–2469 (2012).
8. T. Shibanuma, G. Grinblat, P. Albella, and S. A. Maier, "Efficient third harmonic generation from metal–dielectric hybrid nanoantennas," Nano Lett. **17**(4), 2647–2651 (2017).
9. S. V. Makarov, M. I. Petrov, U. Zywietz, V. Milichko, D. Zuev, N. Lopanitsyna, A. Kuksin, I. Mukhin, G. Zograf, E. Ubyivovk, D. A. Smirnova, S. Starikov, B. N. Chichkov, and Y. S. Kivshar, "Efficient second-harmonic generation in nanocrystalline silicon nanoparticles," Nano Lett. **17**(5), 3047–3053 (2017).

#327087 https://doi.org/10.1364/OE.26.012344
Journal © 2018 Received 27 Mar 2018; revised 25 Apr 2018; accepted 25 Apr 2018; published 30 Apr 2018

Optics EXPRESS

10. T. Schumacher, K. Kratzer, D. Molnar, M. Hentschel, H. Giessen, and M. Lippitz, "Nanoantenna-enhanced ultrafast nonlinear spectroscopy of a single gold nanoparticle," Nat. Commun. **2**, 333 (2011).
11. N. Lapshina, R. Noskov, and Y. Kivshar, "Nanoradar based on nonlinear dimer nanoantenna," Opt. Lett. **37**(18), 3921–3923 (2012).
12. I. S. Maksymov, A. E. Miroshnichenko, and Y. S. Kivshar, "Cascaded four-wave mixing in tapered plasmonic nanoantenna," Opt. Lett. **38**(1), 79–81 (2013).
13. D. Smirnova and Y. S. Kivshar, "Multipolar nonlinear nanophotonics," Optica **3**(11), 1241–1255 (2016).
14. L. Wang, S. Kruk, L. Xu, M. Rahmani, D. Smirnova, A. Solntsev, I. Kravchenko, D. Neshev, and Y. Kivshar, "Shaping the third-harmonic radiation from silicon nanodimers," Nanoscale **9**(6), 2201–2206 (2017).
15. E. Wertz, B. P. Isaacoff, J. D. Flynn, and J. S. Biteen, "Single-molecule super-resolution microscopy reveals how light couples to a plasmonic nanoantenna on the nanometer scale," Nano Lett. **15**(4), 2662–2670 (2015).
16. T. Kalkbrenner, U. Håkanson, A. Schädle, S. Burger, C. Henkel, and V. Sandoghdar, "Optical microscopy via spectral modifications of a nanoantenna," Phys. Rev. Lett. **95**(20), 200801 (2005).
17. H. Eghlidi, K. G. Lee, X.-W. Chen, S. Götzinger, and V. Sandoghdar, "Resolution and enhancement in nanoantenna-based fluorescence microscopy," Nano Lett. **9**(12), 4007–4011 (2009).
18. T. Lohmüller, L. Iversen, M. Schmidt, C. Rhodes, H. L. Tu, W. C. Lin, and J. T. Groves, "Single molecule tracking on supported membranes with arrays of optical nanoantennas," Nano Lett. **12**(3), 1717–1721 (2012).
19. M. F. Garcia-Parajo, "Optical antennas focus in on biology," Nat. Photonics **2**(4), 201–203 (2008).
20. N. Bontempi, K. E. Chong, H. W. Orton, I. Staude, D.-Y. Choi, I. Alessandri, Y. S. Kivshar, and D. N. Neshev, "Highly sensitive biosensors based on all-dielectric nanoresonators," Nanoscale **9**(15), 4972–4980 (2017).
21. B. Wang, F. Dong, Q.-T. Li, D. Yang, C. Sun, J. Chen, Z. Song, L. Xu, W. Chu, Y. F. Xiao, Q. Gong, and Y. Li, "Visible-frequency dielectric metasurfaces for multiwavelength achromatic and highly dispersive holograms," Nano Lett. **16**(8), 5235–5240 (2016).
22. G. Zheng, H. Mühlenbernd, M. Kenney, G. Li, T. Zentgraf, and S. Zhang, "Metasurface holograms reaching 80% efficiency," Nat. Nanotechnol. **10**(4), 308–312 (2015).
23. G. Jönsson, D. Tordera, T. Pakizeh, M. Jaysankar, V. Miljkovic, L. Tong, M. P. Jonsson, and A. Dmitriev, "Solar transparent radiators by optical nanoantennas," Nano Lett. **17**(11), 6766–6772 (2017).
24. R. Guo, M. Decker, F. Setzpfandt, I. Staude, D. N. Neshev, and Y. S. Kivshar, "Plasmonic fano nanoantennas for on-chip separation of wavelength-encoded optical signals," Nano Lett. **15**(5), 3324–3328 (2015).
25. D. Vercruysse, P. Neutens, L. Lagae, N. Verellen, and P. Van Dorpe, "Single asymmetric plasmonic antenna as a directional coupler to a dielectric waveguide," ACS Photonics **4**(6), 1398–1402 (2017).
26. R. Guo, M. Decker, F. Setzpfandt, X. Gai, D. Y. Choi, R. Kiselev, A. Chipouline, I. Staude, T. Pertsch, D. N. Neshev, and Y. S. Kivshar, "High-bit rate ultra-compact light routing with mode-selective on-chip nanoantennas," Sci. Adv. **3**(7), e1700007 (2017).
27. J. M. Geffrin, B. García-Cámara, R. Gómez-Medina, P. Albella, L. S. Froufe-Pérez, C. Eyraud, A. Litman, R. Vaillon, F. González, M. Nieto-Vesperinas, J. J. Sáenz, and F. Moreno, "Magnetic and electric coherence in forward- and back-scattered electromagnetic waves by a single dielectric subwavelength sphere," Nat. Commun. **3**(1), 1171 (2012).
28. Y. H. Fu, A. I. Kuznetsov, A. E. Miroshnichenko, Y. F. Yu, and B. Luk'yanchuk, "Directional visible light scattering by silicon nanoparticles," Nat. Commun. **4**, 1527 (2013).
29. R. Alaee, R. Filter, D. Lehr, F. Lederer, and C. Rockstuhl, "A generalized Kerker condition for highly directive nanoantennas," Opt. Lett. **40**(11), 2645–2648 (2015).
30. A. E. Krasnok, C. R. Simovski, P. A. Belov, and Y. S. Kivshar, "Superdirective dielectric nanoantennas," Nanoscale **6**(13), 7354–7361 (2014).
31. W. Liu, J. Zhang, B. Lei, H. Ma, W. Xie, and H. Hu, "Ultra-directional forward scattering by individual core-shell nanoparticles," Opt. Express **22**(13), 16178–16187 (2014).
32. W. Liu, "Ultra-directional super-scattering of homogenous spherical particles with radial anisotropy," Opt. Express **23**(11), 14734–14743 (2015).
33. R. R. Naraghi, S. Sukhov, and A. Dogariu, "Directional control of scattering by all-dielectric core-shell spheres," Opt. Lett. **40**(4), 585–588 (2015).
34. W. Liu, B. Lei, J. Shi, and H. Hu, "Unidirectional superscattering by multilayered cavities of effective radial anisotropy," Sci. Rep. **6**(1), 34775 (2016).
35. R. W. Ziolkowski, "Using huygens multipole arrays to realize unidirectional needle-like radiation," Phys. Rev. X **7**(3), 031017 (2017).
36. G. W. Lu, Y. W. Wang, R. Y. Chou, H. M. Shen, Y. B. He, Y. Q. Cheng, and Q. H. Gong, "Directional side scattering of light by a single plasmonic trimer," Laser Photonics Rev. **9**(5), 530–537 (2015).
37. D. Vercruysse, Y. Sonnefraud, N. Verellen, F. B. Fuchs, G. Di Martino, L. Lagae, V. V. Moshchalkov, S. A. Maier, and P. Van Dorpe, "Unidirectional side scattering of light by a single-element nanoantenna," Nano Lett. **13**(8), 3843–3849 (2013).
38. J. Li, N. Verellen, D. Vercruysse, T. Bearda, L. Lagae, and P. Van Dorpe, "All-dielectric antenna wavelength router with bidirectional scattering of visible light," Nano Lett. **16**(7), 4396–4403 (2016).
39. Z.-Y. Jia, J.-N. Li, H.-W. Wu, C. Wang, T.-Y. Chen, R.-W. Peng, and M. Wang, "Dipole coupling and dual Fano resonances in a silicon nanodimer," J. Appl. Phys. **119**(7), 074302 (2016).
40. J. Tian, Q. Li, Y. Yang, and M. Qiu, "Tailoring unidirectional angular radiation through multipolar interference in a single-element subwavelength all-dielectric stair-like nanoantenna," Nanoscale **8**(7), 4047–4053 (2016).

Optics EXPRESS

41. T. Shibanuma, T. Matsui, T. Roschuk, J. Wojcik, P. Mascher, P. Albella, and S. A. Maier, "Experimental demonstration of tunable directional scattering of visible light from all-dielectric asymmetric dimers," ACS Photonics **4**(3), 489–494 (2017).
42. M. Peter, A. Hildebrandt, C. Schlickriede, K. Gharib, T. Zentgraf, J. Förstner, and S. Linden, "Directional emission from dielectric leaky-wave nanoantennas," Nano Lett. **17**(7), 4178–4183 (2017).
43. T. Kaelberer, V. A. Fedotov, N. Papasimakis, D. P. Tsai, and N. I. Zheludev, "Toroidal dipolar response in a metamaterial," Science **330**(6010), 1510–1512 (2010).
44. A. B. Evlyukhin, T. Fischer, C. Reinhardt, and B. N. Chichkov, "Optical theorem and multipole scattering of light by arbitrarily shaped nanoparticles," Phys. Rev. B **94**(20), 205434 (2016).
45. T. Feng, Y. Xu, W. Zhang, and A. E. Miroshnichenko, "Ideal magnetic dipole scattering," Phys. Rev. Lett. **118**(17), 173901 (2017).
46. N. Papasimakis, V. A. Fedotov, V. Savinov, T. A. Raybould, and N. I. Zheludev, "Electromagnetic toroidal excitations in matter and free space," Nat. Mater. **15**(3), 263–271 (2016).
47. P. Grahn, A. Shevchenko, and M. Kaivola, "Electromagnetic multipole theory for optical nanomaterials," New J. Phys. **14**(9), 093033 (2012).
48. I. M. Hancu, A. G. Curto, M. Castro-López, M. Kuttge, and N. F. van Hulst, "Multipolar interference for directed light emission," Nano Lett. **14**(1), 166–171 (2014).
49. A. I. Kuznetsov, A. E. Miroshnichenko, M. L. Brongersma, Y. S. Kivshar, and B. Luk'yanchuk, "Optically resonant dielectric nanostructures," Science **354**(6314), 6314 (2016).
50. Z.-J. Yang, R. Jiang, X. Zhuo, Y.-M. Xie, J. Wang, and H.-Q. Lin, "Dielectric nanoresonators for light manipulation," Phys. Rep. **701**, 1–50 (2017).
51. F. Aieta, M. A. Kats, P. Genevet, and F. Capasso, "Multiwavelength achromatic metasurfaces by dispersive phase compensation," Science **347**(6228), 1342–1345 (2015).
52. J. Xiang, J. Li, H. Li, C. Zhang, Q. Dai, S. Tie, and S. Lan, "Polarization beam splitters, converters and analyzers based on a metasurface composed of regularly arranged silicon nanospheres with controllable coupling strength," Opt. Express **24**(11), 11420–11434 (2016).
53. R. Paniagua-Domínguez, Y. F. Yu, E. Khaidarov, S. Choi, V. Leong, R. M. Bakker, X. Liang, Y. H. Fu, V. Valuckas, L. A. Krivitsky, and A. I. Kuznetsov, "A metalens with a mear-unity numerical aperture," Nano Lett. **18**(3), 2124–2132 (2018).
54. E. Khaidarov, H. Hao, R. Paniagua-Domínguez, Y. F. Yu, Y. H. Fu, V. Valuckas, S. L. K. Yap, Y. T. Toh, J. S. K. Ng, and A. I. Kuznetsov, "Asymmetric nanoantennas for ultrahigh angle broadband visible light bending," Nano Lett. **17**(10), 6267–6272 (2017).
55. J. Xiang, J. Li, Z. Zhou, S. Jiang, J. Chen, Q. Dai, S. L. Tie, S. Lan, and X. H. Wang, "Manipulating the orientations of the electric and magnetic dipoles induced in silicon nanoparticles for multicolor display," Laser Photonics Rev. **0**, 1800032 (2018).
56. C. Ma, J. Yan, Y. Huang, and G. W. Yang, "Directional Scattering in a Germanium Nanosphere in the Visible Light Region," Adv. Opt. Mater. **5**(24), 1700761 (2017).
57. Y. Yang, A. E. Miroshnichenko, S. V. Kostinski, M. Odit, P. Kapitanova, M. Qiu, and Y. S. Kivshar, "Multimode directionality in all-dielectric metasurface," Phys. Rev. B **95**(16), 165426 (2017).

1. Introduction

It is well known that the operating frequency of an antenna depends strongly on the dimension of the antenna. The smaller the antenna, the higher is the supporting frequency. In the past two decades, the size of antennas is greatly reduced owing to the significant advance in micro- and nano-processing technology and near-field optical microscopy [1]. Antennas with micro- and even nanometer sizes, which operate at optical frequencies, have be successfully fabricated. So far, antennas of nanometer sizes have been widely applied in solar cells [2–4], optical absorption and detection [5–7], nonlinear optics [8–14], micro- and nano-display and imaging [15–17], biological sensors [18–20], nano-holography [21,22], temperature control [23] and optical interconnectors [24–26].

Antennas working in the long wavelength range are generally constructed by metals. Due to the large Ohmic losses of metals in the visible light spectrum, naono-antennas composed of dielectric and semiconductor nanoparticles/nanostructures with large refractive indices have become the focus of many studies because they support strong electric and magnetic resonances in the visible to near infrared spectral range.

One of the most important properties of nano-antennas is the directivity of the radiation. Much effort has been devoted to the design of nano-antennas with ultrahigh directivity. On the other hand, much attention has been paid to the side radiation of nano-antennas. However, it remains a big challenge to realize nano-antennas whose radiation directivity and direction can be simultaneously manipulated.

Optics EXPRESS

For dielectric and semiconductor nanoparticles, it has been demonstrated that the constructive interference between the induced electric and magnetic dipole (ED and MD) may lead to the enhanced scattering in the forward direction and suppressed scattering in the backward direction at the wavelength where the first Kerker's condition is satisfied [27,28]. The situation is reversed at the wavelength where the second Kerker's condition is satisfied. This kind of directional scattering is quite useful in the design of all-dielectric nano-antennas. Apart from the interference between electric and magnetic dipoles, it was shown recently that the interference between the ED and electric quadrupole (EQ) can lead to highly directional radiation at the wavelength where the generalized Kerker's condition is fulfilled [29]. In addition to the highly directional radiation, the directivity of the radiation is also significantly improved. It implies that the interference between the low-order and high-order electromagnetic modes can be employed to shape the radiation directivity of nano-antennas. It was demonstrated that nano-antennas with super-directivity can be achieved by incorporating more high-order modes into the interference [30–34]. More interestingly, nano-antennas which produce needle radiation can be realized by using an array composed of hundreds or even thousands of dipoles [35].

Basically, an effective way to control the radiation direction of a nano-antenna relies on the interference of electric and magnetic modes of different orders, leading to the so-called side scattering. So far, side scattering was firstly achieved by exploiting the interference of two parallel and spatially-separated electric dipoles [36,37]. It was also realized by utilizing the interference of the ED parallel to the incident wave, which is induced by the asymmetric nanostructure, and the MD/EQ perpendicular to the incident wave [38]. In general, side scattering can be achieved by an asymmetric structure with respect to the incident wave [39–42].

In order to realize the control and manipulation of the radiation direction and directivity of a nano-antenna, it is necessary to excite as many electric and magnetic resonances as possible. For plasmonic nano-antennas, electric modes of various orders and low-order magnetic modes can be used. However, it is difficult to excite high-order magnetic modes. In comparison, electric and magnetic modes of different orders can be readily excited in dielectric nanostructures, offering more possibilities to engineer the radiation direction and directivity of a nano-antenna.

As far as the interference of two electromagnetic modes is concerned, both the amplitudes and phases of these two modes need to be taken into account. When analyzing the forward and backward scattering of a silicon (Si) nanosphere (NS), its total scattering is generally decomposed into the contributions of ED, MD and multipoles based on Mie theory. The ED and MD are represented by the expansion coefficients of b_1 and a_1, respectively. For a Si NS with d = 150 nm, the first and second Kerker's conditions are approximately satisfied at the wavelengths of 648 and 575 nm where the amplitudes of the ED and MD are the same (i.e., $a_1 = b_1$) (see Section A1, Appendix). If we examine the phase difference between the ED and MD of the Si NS, however, the phase differences at these two wavelengths are found to be 0 and 2.09. As a result, the backward scattering is completely suppressed at 648 nm where the phase difference is close to 0. In sharp contrast, the forward scattering of the Si NS is still appreciable at 575 nm because the phase difference is far from π. This example indicates the importance of phase difference in the interference of two electromagnetic modes. Similar behavior is also observed in germanium (Ge) NS (see Section A1, Appendix). It implies that the Kerker's condition is not easily satisfied in dielectric NSs without specially designed structures.

In this article, we proposed an all-silicon-based nano-antenna capable of realizing both wavelength and polarization demultiplexing which are considered as the key components in the integrated optical circuits. We demonstrated numerically that radiation with adjustable direction and high directivity and can be realized in such a nano-antenna which is compatible with the current fabrication technology of Si chips.

Optics EXPRESS

The structure of the nano-antenna, which acts as not only a wavelength demultiplexer but also a polarization demultiplexer, is schematically shown in Fig. 1. It is composed of two Si cuboids with the same length and height but different widths. When the nano-antenna is excited with an incident wave whose polarization is perpendicular to the long side of the Si cuboids, an ED, a MD and a magnetic quadrupole (MQ) will be induced in each Si cuboid. In addition, the coupling between the two Si cuboids will create an ED component parallel to the incident wave because of the asymmetric structure of the nano-antenna (i.e., the widths of the two Si cuboids are different). The appearance of the ED component parallel to the incident wave (i.e., ED_z) makes it possible to manipulate the radiation direction of the nano-antenna. In addition, the EQ and MQ of each Si cuboid offer the opportunity for further engineering the radiation directivity through the interference with ED and MD.

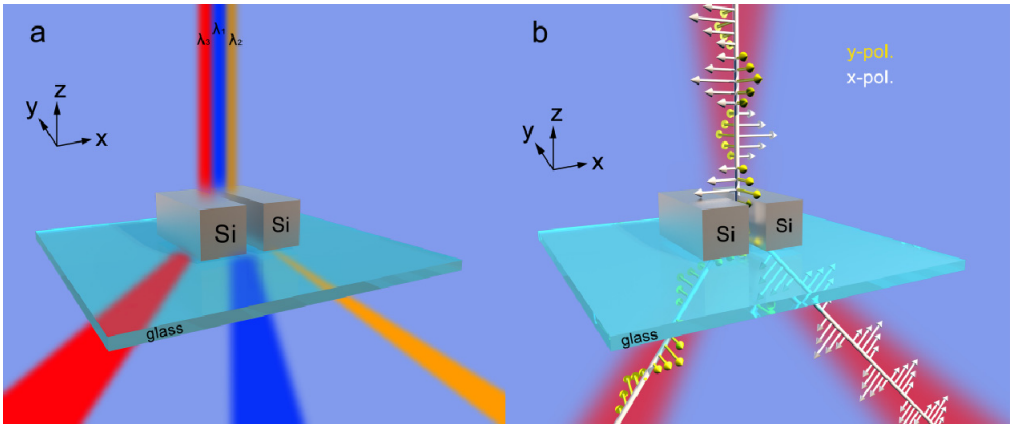

Fig. 1. Schematic showing the structure of the proposed nano-antenna which functions as a wavelength (a) and a polarization (b) demultiplexer.

2. Theoretical and numerical methods

The interaction of a nano-antenna with the incident light can induce the change in the charge and current density distributions of the nano-antenna. The polarization of charge and the conduction of current lead to the scattering of the incident light. In order to analyze the radiation pattern of the scattered light more quantitatively, one need to know the polarization charge or displacement current of different spatial orientations in the scattering field of the nano-antenna. In general, one can use multipolar moments or multipolar coefficients to describe the charge and current density distributions in space. For a simple antenna, one can describe the current density in *x*, *y*, and *z* directions by using the three components of the ED (i.e., ED_x, ED_y, and ED_z). For a more complex antenna, the multipole expansion method need to be used to ensure the correctness of the moment expansion. At present, there are two types of multipole expansion. In a Cartesian coordinate, the multipole expansion of ED, MD, EQ, and MQ can be expressed as follows [43–46]:

$$\mathrm{ED} = \frac{1}{-i\omega}\int \mathrm{j} d^3 r, \tag{1}$$

$$\mathrm{MD} = \frac{1}{2c} = \int (\mathrm{r}\times \mathrm{j}) d^3 r, \tag{2}$$

$$\mathrm{EQ}_{\alpha\beta} = \frac{1}{-i2\omega} = \int \left[r_\alpha j_\beta + r_\beta j_\alpha - \frac{2}{3}(r\cdot j)\delta_{\alpha\beta} \right] d^3 r. \tag{3}$$

Optics EXPRESS

$$\mathrm{MQ}_{\alpha\beta} = \frac{1}{3c}\int\left[(\mathrm{r}\times\mathrm{j})_{\alpha} r_{\beta} + (\mathrm{r}\times\mathrm{j})_{\beta} r_{\alpha}\right] d^3 r. \tag{4}$$

Here, c is the speed of light in vacuum, α and β represent the Cartesian coordinate components x, y, and z. The current density is given by:

$$\mathrm{J}(\mathrm{r}) = -i\omega\varepsilon_0\left[\varepsilon_{\mathrm{r}}(\mathrm{r}) - \varepsilon_{\mathrm{r,d}}\right]\mathrm{E}(\mathrm{r}). \tag{5}$$

Alternatively, the multipole expansion can be performed in a spherical coordinate in which the coefficients of ED and MD can be described as follows [47]:

$$\begin{aligned} a_{\mathrm{E}}(l,m) = {} & \frac{(-\mathrm{i})^{l-1}k^2\eta O_{lm}}{E_0[\pi(2\mathrm{l}+1)]^{1/2}}\int \exp(-\mathrm{i}m\phi)\{[\psi_l(kr)+\psi_l''(kr)]\times P_l^m(\cos\theta)\hat{\hat{\mathbf{r}}}\cdot J(r). \\ & + \frac{\psi_l'(kr)}{kr}[\tau_{lm}(\theta)\hat{\theta}\cdot J(r) - \mathrm{i}\pi_{lm}(\theta)\hat{\phi}\cdot J(r)]\}\,\mathrm{d}^3 r \end{aligned} \tag{6}$$

$$\begin{aligned} a_{\mathrm{M}}(l,m) = {} & \frac{(-\mathrm{i})^{l-1}k^2\eta O_{lm}}{E_0[\pi(2\mathrm{l}+1)]^{1/2}}\int \exp(-\mathrm{i}m\phi) j_l(kr) \\ & \times[\tau_{lm}(\theta)\hat{\theta}\cdot J(r) + \mathrm{i}\pi_{lm}(\theta)\hat{\phi}\cdot J(r)]\}\,\mathrm{d}^3 r \end{aligned} \tag{7}$$

Here, $\Psi_l(kr) = krj_l(kr)$ is Riccati–Bessel functions, $\Psi' l\ (kr)$ and$\Psi''\ l\ (kr)$ are the first and second derivatives with respect to the parameter of kr. $Pm\ l$ is Legendre polynomials, O_{lm},$\tau_{lm}(\theta)$, $\pi_{lm}(\theta)$ are related parameters.

The coefficients of the multipole expansion described in this work were calculated by using a commercial software developed by the COMSOL Co., Ltd (https://cn.comsol.com/). It is a numerical simulation software based on the finite element (FE) method (Multiphysics v5.3a.). The numerical simulations were performed in a sphere whose diameter was chosen to be about 1.5 times the wavelength of the incident light. Outside the sphere, a perfectly matched layer (PML) was used to absorb all the outgoing radiation. The nano-antenna was placed at the center of the sphere. The mesh generation was completed by using the built-in algorithm of the program, which created tetrahedral meshes. In the case of antenna array, periodic boundary conditions were applied in the lateral directions (x and y) of the system to simulate an infinite Cartesian lattice. In the vertical directions (z direction), several ports were used to collect the defected light of diffracted orders both in transmission and reflection. One of them (on the substrate side) was used to excite the system with a plane wave.

The three-dimensional (3D) far-field scattering intensity distributions were calculated by using the finite-difference time-domain (FDTD) technique developed by Lumerical Ltd (https://www.lumerical.com/). No obvious difference was found in simulation results obtained by using the FE (Multiphysics, COMSOL Co., Ltd.) and FDTD (FDTD solution, Lumerical Ltd.) methods

3. Results and discussion

3.1 Influence of amplitude and phase on the radiation pattern

Basically, the radiation pattern of a nano-antenna is determined by the interference between the moments obtained from the multipole expansion in a Cartesian coordinate or the interference between the coefficients obtained from the multipole expansion in a spherical coordinate. For example, the interference between an ED and a MD perpendicular to each other with equal amplitude and a phase difference of 0 will lead to the complete suppression of the backward scattering (i.e., the so-called first Kerker's condition). If the phase difference between the two dipoles is π, then a complete suppression of the forward scattering is observed (i.e., the so-called second Kerker's condition).

Optics EXPRESS

In order to fulfil the first and second Kerker's conditions, there are two requirements. First, the amplitudes of the two dipoles must be equal. Second, their phase difference should be 0 or π. In Fig. 2(a), we show the evolution of the two-dimensional (2D) scattering pattern resulting from the interference of two identical dipoles perpendicular to each other with increasing phase difference (δ). It can be seen that the backward scattering increases with increasing phase difference and it becomes equal to the forward scattering when the phase difference is increased to π/2. In addition to the phase difference, the scattering pattern is also affected by the amplitudes of the two dipoles. In Fig. 2(b), we present the evolution of the 2D scattering pattern resulting from two dipoles oscillating in phase when the ratio of their amplitudes (r) is increased. One can see clearly the increase of backward scattering when the ratio of their amplitudes is increased. This simple example indicates that the scattering pattern is determined not only by the amplitudes of the two dipoles but also by their phase difference.

In the case when the two dipoles have similar amplitudes, the phase difference between them plays a dominant role in determining the radiation pattern. If we consider the interference between an ED (or a MD) and an EQ (or a MQ) (i.e., the so-called generalized Kerker's condition [29]), the phase difference between the dipole and the quadrupole should be π/2 or 3π/2 in order to achieve a complete forward or backward scattering [48]. Similar conditions must be satisfied when the interference between high-order modes is considered.

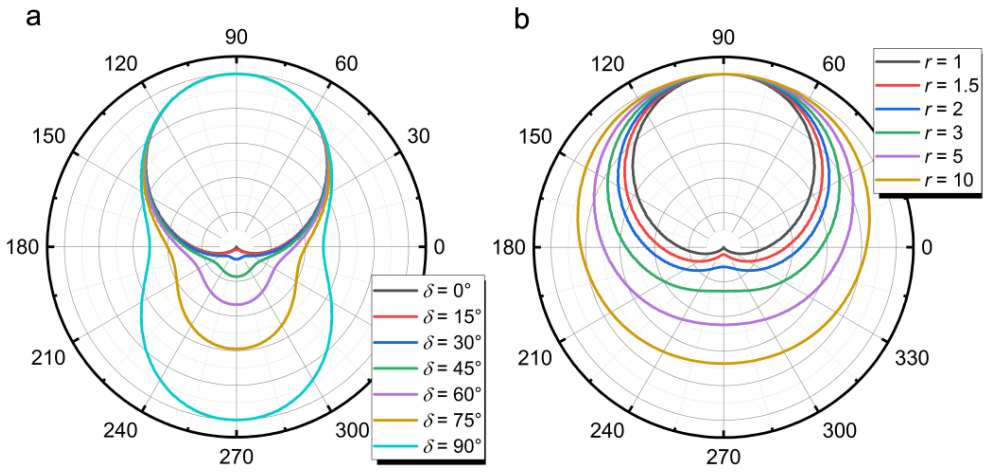

Fig. 2. (a) Evolution of the 2D scattering pattern resulting from two identical dipoles perpendicular to each other with increasing phase difference. (b) Evolution of the 2D scattering pattern resulting from two dipoles oscillating in phase with increasing ratio of their amplitudes.

In general, we need to consider not only the amplitudes of the two interacting multipoles but also their phase difference in order to manipulate the radiation pattern. In the design of nano-antennas, we need to create a dipole which possesses not only a large amplitude but also an orientation parallel to the propagation direction of the incident wave. The phase difference between this dipole and the dipole perpendicular to the incident wave should be close to 0 or π, leading to the so-called side scattering. In this way, we can manipulate the radiation direction of the nano-antenna. Based on this, we can exploit the interference between the dipole and high-order multipole to shape the directivity of the radiation.

Owing to its large refractive index, Si nanoparticles of different shapes such as nanospheres, nanopillars, and nanodisks have been widely used to construct nanoscale photonic devices with different functions [49–52]. Here, we chose two Si cuboids with the same length and height but with different widths to construct the nano-antenna, as schematically shown in Fig. 1. In practice, such a nano-antenna can be fabricated on a quartz substrate by using the combination of wafer bonding, electron beam lithography and focused

Optics EXPRESS

ion etching. As compared with the nano-antennas proposed previously [40], the nano-antenna proposed in this work is easier to be fabricated because the constituent Si cuboids have the same height. When the polarization of the incident wave is perpendicular to the long side of the Si cuboids, the magnetic field parallel to the long side can excite the MQ in each Si cuboid. The interference between the ED and the MQ of the Si cuboid can be exploited to improve the directivity of the radiation.

We first examine the electric and magnetic multipoles excited in each Si cuboid by the incident wave whose polarization is perpendicular to the long side of the Si cuboids, as shown in Fig. 3. The multipole expansion of the total scattering of a single Si cuboid was performed in a spherical coordinate. In Fig. 3(a), we show the multipole expansion of the scattering spectrum carried out for the left Si cuboid in the nano-antenna whose length, height and width are designed to be l_1 = 400 nm, h_1 = 220 nm, and w_1 = 120 nm, respectively. One can see two scattering peaks in the total scattering spectrum. The scattering peak located at ~784 nm arises from the MD of the Si cuboid while that located at ~642 nm results from the ED and the MQ of the Si cuboid. The electric field distribution at the ED resonance and the magnetic field distributions at the MD and MQ resonances are shown in the insets of Fig. 3(a).

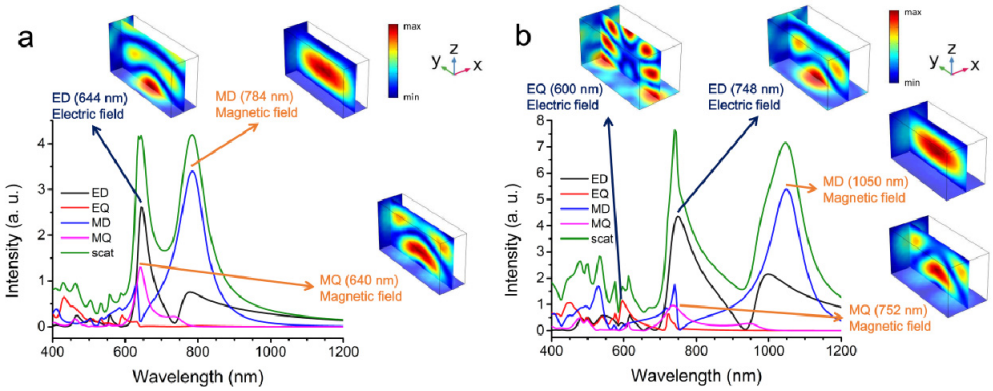

Fig. 3. Multipole expansion of the total scattering of a single Si cuboid with w_1 = 120 nm (a) and w_2 = 200 nm (b). The electric field distributions at the ED and EQ resonances and the magnetic field distributions at the MD and MQ resonances are presented as insets.

Similarly, the scattering spectrum of the right Si cuboid, whose length, height, and width are designed to be l_1 = 400 nm, h_1 = 220 nm, and w_1 = 200 nm, can also be decomposed into the contributions of the ED, MD, and MQ, as shown in Fig. 3(b). As compared with the left one, the two major scattering peaks are red shifted. The scattering peak corresponding to the MD is red shifted to ~1050 nm while that originating from the ED and MQ is red shifted to ~750 nm. Moreover, the scattering peak corresponding to the EQ becomes apparent at ~600 nm. The electric field distributions at the ED and EQ resonances and the magnetic field distributions at the MD and MQ resonances are presented in the insets of Fig. 3(b).

In principle, the MQ in each Si cuboid is induced by the retardation effect and it is parallel to the *yz* plane (MQ_{yz}). Such a MQ is still present when the coupling between two Si cuboids is introduced. It will be demonstrated later that the MQ of the Si cuboids plays a crucial role in improving the directivity of the radiation.

3.2 Radiation direction controlled by the interference of electric and magnetic dipoles

We performed multipole expansion for the total scattering spectrum of the nano-antenna in both a spherical and a Cartesian coordinate, as shown in Fig. 4(a) and Fig. 4(b). It can be seen that the ED and MQ in the individual Si cuboid are retained in the nano-antenna. The coupling between the two Si cuboids has negligible influence on these modes, as evidenced in the insets of Fig. 4(a) where the electric and magnetic field distributions of these modes are

Optics EXPRESS

presented. Therefore, these modes can be employed to manipulate the radiation pattern of the nano-antenna.

Since the widths of the two Si cuboids are chosen to be different, the nano-antenna appears to be asymmetric when the polarization of the incident wave is along the *x* direction. In this case, the electric field inside the nano-antenna is also asymmetric, creating an EQ component on the *xz* plane (i.e., EQ_{xz}). In addition, the ED and MQ of the nano-antenna are tilted to some extent, generating new components of ED_z and MQ_{xy}. From the multipole expansion of the scattering spectrum of the nano-antenna in the Cartesian coordinate [see Fig. 4(b)], the electric and magnetic modes that contribute mainly to the total scattering of the nano-antenna include ED_x, ED_z, MD_y, EQ_{xz}, and MQ_{yz}. Therefore, we will discuss in the following how the interference of these electric and magnetic modes can be utilized to manipulate the radiation direction and to shape the radiation directivity. In this case, the nano-antenna is symmetric with respect to the magnetic field of the incident wave. As a result, the magnetic field distribution inside the nano-antenna is symmetric with respect to the *xz* plane, so is the radiation pattern of the nano-antenna.

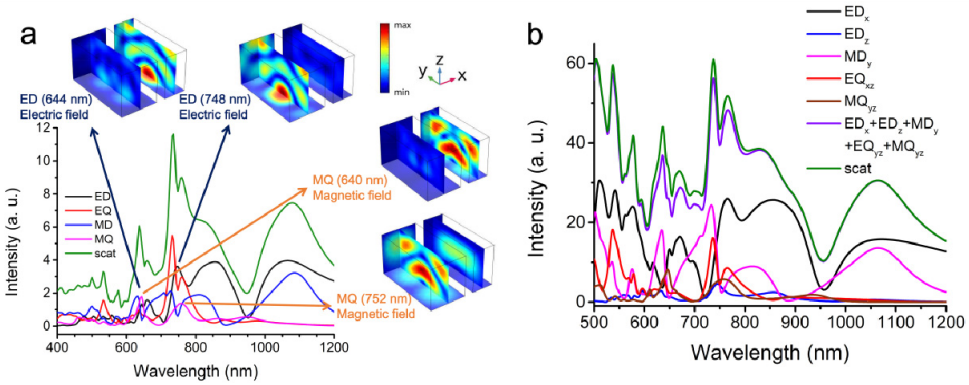

Fig. 4. Multipole expansion of the total scattering spectrum of the nano-antenna in a spherical (a) and a cartesian (b) coordinate. The electric field distributions at the ED resonances (644 and 748 nm) and the magnetic field distributions at the MQ resonances (640 and 752 nm) are shown in the insets of (a). In (b), we present the electric and magnetic modes with relative large amplitudes (ED_x, ED_z, MD_y, EQ_{xz}, MQ_{yz}) which determine the radiation direction and directivity of the nano-antenna.

In order to gain a deep insight into the interference between different dipoles and its effect on the radiation pattern, we present the 3D and 2D radiations of the MD_y, ED_z and ED_x, which are the major contributions to the radiation of the nano-antenna, in Fig. 5. As illustrated in Fig. 5, the deflection of the radiation along the *x* direction (i.e., side scattering) is mainly governed by the interference between MD_y and ED_z. In this case, the phase difference plays a dominant role because they have similar amplitudes. If the phase difference between them is in the region of $(-\pi/2, \pi/2)$, the two modes are considered as in-phase and the radiation is deflected to the $+x$ direction. In comparison, the deflection of the radiation to the $-x$ direction occurs when the two modes are out-of-phase (i.e., the phase difference is in the regions of $(-\pi, -\pi/2)$ and $(-\pi/2, \pi)$. Similarly, the radiation in the *z* direction (i.e., forward and backward scattering) is determined by the interference between MD_y and ED_x, as schematically shown in Fig. 5. The phase difference also plays a crucial role in determining the radiation direction.

Optics EXPRESS

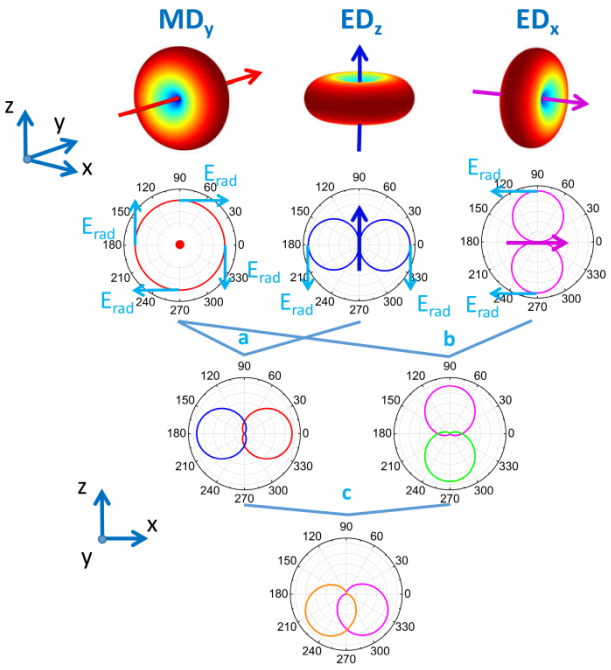

Fig. 5. Schematic showing the 3D (first row) and 2D (second row) radiation patterns of MD_y, ED_z, and ED_x induced in the nano-antenna. Also shown are the schematic radiation pattern resulting from the interference between MD_y and ED_z and that resulting from the interference between MD_y and ED_x (third row). The schematic radiation pattern of the nano-antenna, which is determined by the interference of these three modes, is presented in the fourth row.

As discussed above, the deflection of the radiation is governed mainly by phase difference between MD_y and ED_z. In Fig. 6(a), we show the wavelength dependence of the phase difference between these two modes and indicate the wavelengths at which the phase differences are equal to 0 and π. The two modes are considered as in-phase when the phase difference between them is in the region of [-π/2, π/2]. In this case, the radiation is deflected to the + *x* direction and the maximum deflection is achieved at the wavelength where the phase difference is 0. Similarly, the two modes are considered as out-of-phase when the phase difference is in the region of [-π, -π/2] or [π/2, π]. In this case, the radiation is deflected to the –*x* direction and the maximum deflection angle is observed at the wavelength where the phase difference is π. In Fig. 6(b), we present the wavelength dependence of the maximum radiation angle obtained by using the FDTD simulation. It can be seen that the maximum deflection angle of ~23° to the + *x* direction is achieved at ~583 nm where the phase difference between MD_y and ED_z is close to 0. Accordingly, the maximum deflection angle of ~35° to the -*x* direction is achieved at ~680 nm where the phase difference between MD_y and ED_z is close to -π. The simulation results are in good agreement with the theoretical predictions based on the calculation of the phase difference.

In Fig. 6(c), we plot MD_y, ED_x, and ED_z as vectors whose lengths represent the amplitudes and the orientations represent the phases. The phase difference between two modes can be readily found by the angle between the two vectors. It can be seen that the amplitude of MD_y is maximum at 583 nm and the phase difference between MD_y and ED_z is 0. As a result, the largest deflection angle to the + *x* direction is achieved at this wavelength. Similarly, another maximum of MD_y is obtained at 680 nm and the phase difference between MD_y and ED_z is -π. Thus, the largest deflection angle to the –*x* direction is observed at this wavelength. Although the phase difference between MD_y and ED_z is close to 0 at ~751 nm, the deflection of the radiation is not significant because the amplitude of ED_x is much larger

Optics EXPRESS

than that of MD_y. Similar situation is observed at ~888 nm where the phase difference between MD_y and ED_z is close to -π. Therefore, the following two conditions need to be fulfilled in order to achieve the largest radiation deflection. First, MD_y should be the dominant mode with larger amplitude. Second, the phase difference between MD_y and ED_z should be close to 0 or ± π.

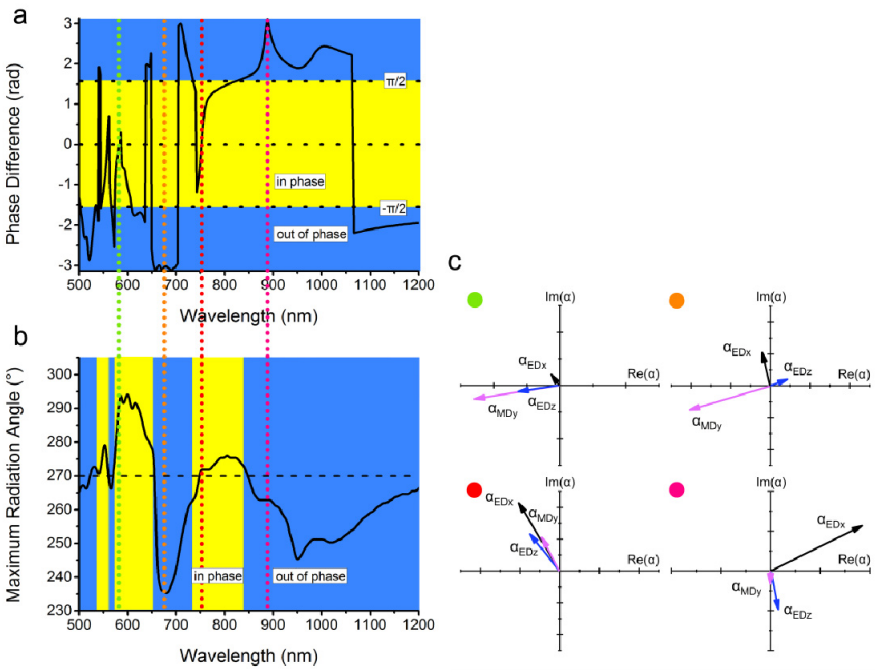

Fig. 6. (a) Phase difference between MD_y and ED_z as a function of wavelength. (b) Deflection angle of the radiation as a function of wavelength. (c) Vector diagrams for MD_y, ED_z, and ED_x.

3.3 Radiation directivity engineered by the interference of dipoles and quadrupoles

Now we examine the interference between dipoles and quadrupoles and its influence on the radiation directivity, as schematically shown in Fig. 7. Here, we consider only the quadrupoles (i.e., MQ_{yz} and EQ_{xz}) with relatively large amplitudes, as shown in Fig. 5(b). In Fig. 7(a), we show the 3D and 2D radiation patterns of ED_x and MQ_{yz} with similar strengths and the radiation pattern resulting from the interference of these two modes. It can be seen that the interference between ED_x and MQ_{yz} will lead to the radiation only in the *z* direction when the phase difference between them is equal to -π/2 or 3π/2. In contrast, a phase difference of + π/2 or −3π/2 will result in the radiation only in the *y* direction (not shown). The former is good to the radiation directivity while the latter is not. By deliberately adjusting the structure parameters of the nano-antenna, we can make the radiation peak originating from the interference of MD_y and ED_z coincide with that originating from the interference of ED_x and MQ_{yz}, leading to a nano-antenna with controllable radiation direction and super-directivity. Similarly, the interference between MD_y and EQ_{xz} can also be exploited to improve or deteriorate the radiation directivity, depending strongly on the phase difference between them. When the phase difference between is close to + π/2, an improvement in radiation directivity can be achieved, as shown in Fig. 7(b).

Optics EXPRESS

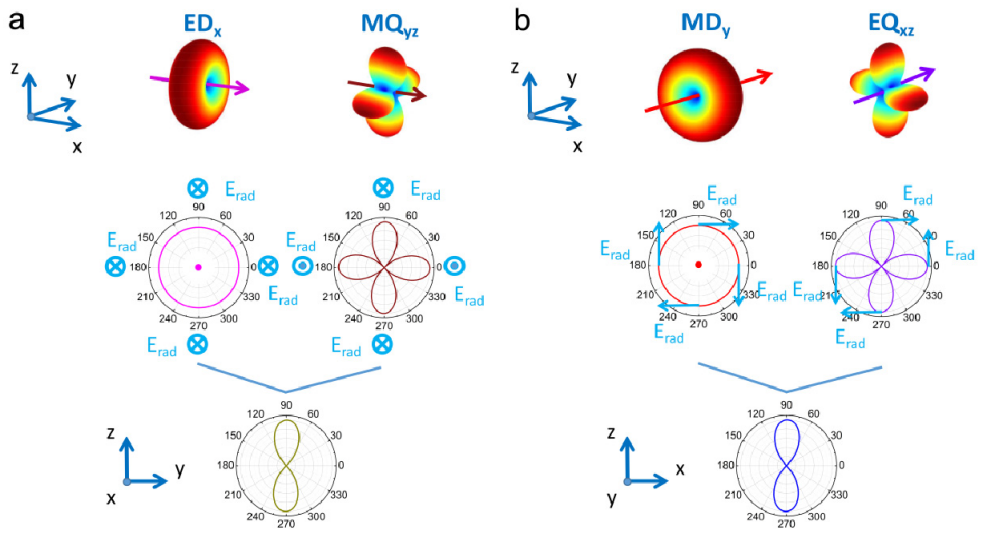

Fig. 7. (a) Schematic showing the 3D and 2D radiation patterns of ED_x and MQ_{yz} and the radiation pattern resulting from the interference of these two modes. (b) Schematic showing the 3D and 2D radiation patterns of MD_y and EQ_{xz} and the radiation pattern resulting from the interference of these two modes.

Now we discuss in detail the influence of the quadrupoles on the radiation directivity. The radiation directivity of a nano-antenna is usually characterized by a parameter D, which is defined as the ratio of the maximum radiation power on the surface of a sphere in the far field to the averaged value [30]:

$$D = \frac{P(\theta,\varphi)_{\max}}{P(\theta,\varphi)_{av}}. \tag{8}$$

Here, the averaged power on the surface of the sphere is given by:

$$P(\theta,\varphi)_{av} = \frac{1}{4\pi}\int_{\varphi=0}^{\varphi=2\pi}\int_{\theta=0}^{\theta=\pi} P(\theta,\varphi)\sin\theta d\theta d\varphi \ (\mathrm{W\,sr^{-1}}). \tag{9}$$

In Fig. 8(a), we present the wavelength dependence of the parameter D calculated for the nano-antenna. The corresponding wavelength dependence of the $HPBW_y$, which is the full width at half of the maximum power in the y direction, is also presented. It can be seen that the best directivity is achieved at ~405 nm where $HPBW_y$ has the minimum value of 35° while D has the maximum value of 14.21. As discussed above, the interference between ED_x and MQ_{yz} can be employed to engineer the radiation pattern of the nano-antenna. In case of forward scattering, the interference between them can improve the radiation directivity of the nano-antenna when the phase difference between them is equal to $-\pi/2$. As can be seen from the vector diagrams shown in Figs. 8(b) and 8(c), the phase differences between ED_x and MQ_{yz} are close to $-\pi/2$ at 640 and 752 nm. As a result, the $HPBW_y$ reaches its minimum at these two wavelengths. Accordingly, the parameter D has maximum values at these two wavelengths, implying significantly improved radiation directivity. In Fig. 8(d), the radiation directivity is not good although the phase difference between ED_x and MQ_{yz} is close to $\pi/2$. The major reason for the deterioration of the radiation directivity is the small amplitude of ED_x. In addition, the amplitudes of MD_y and EQ_{xz} are relatively large and their phase difference is large than 0 but not close to $\pi/2$, deteriorating the radiation directivity.

At 526 and 712 nm [see Figs. 8(e) and 8(f)], MD_y and EQ_{xz} possess large amplitudes and their phase difference is close to $\pi/2$. Consequently, we can observe the maximum values of

Optics EXPRESS

parameter *D* at these two wavelengths. At 653 nm [see Fig. 8(g)], the radiation directivity is deteriorated because the phase difference between MD_y and EQ_{xz} is close to 0.

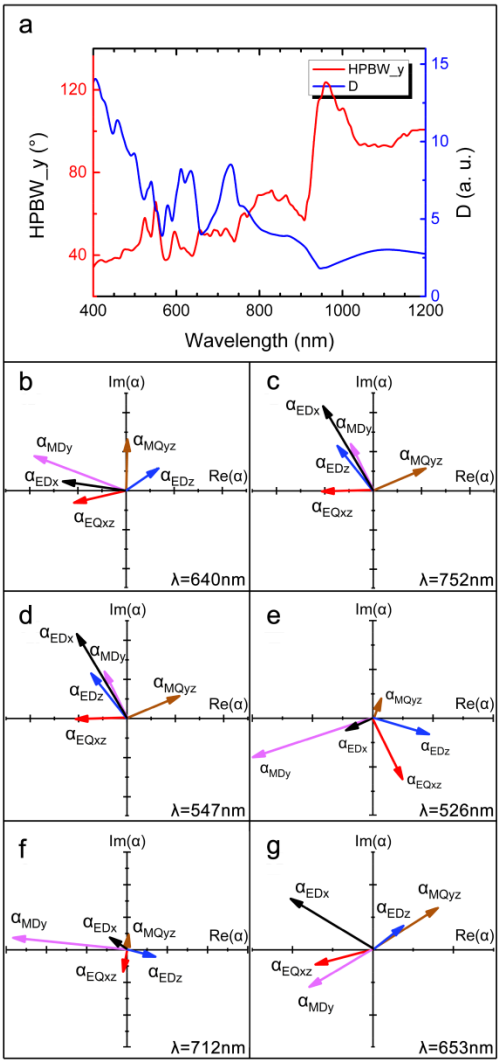

Fig. 8. (a) Wavelength dependences of $HPBW_y$ and D. (b)-(g) Vector diagrams plotted for ED_x, MD_y, MQ_{yz} and EQ_{xz} at different wavelengths.

3.4 Radiation directivity engineered by the interference of dipoles and quadrupoles

We have simulated the wavelength dependence of the maximum radiation angle of the nano-antenna, from which the deflection angle can be deduced, by using the FDTD method, as shown in Fig. 9(a). The largest deflection angle of ~25° to the + *x* direction is observed at ~600 nm while the largest deflection angle of ~36° to the –*x* direction is observed at ~680 nm. At 950 nm, a large deflection angle of ~25° is also observed. However, the radiation pattern at long wavelengths is dominated by dipoles and its directivity is not as good as that at short wavelengths where quadrupoles can interact with dipoles effectively. The 3D and 2D radiation patterns at 405, 600, and 680 nm are presented in Figs. 9(b)-9(g). It is apparent that the wavelength dependence of the radiation direction (or deflection angle) can be employed to realize wavelength demultiplexing. At 600 nm, the radiation is deflected to the + *x* direction

Optics EXPRESS

by ~25° with a good directivity (D ~6.7). The radiation is deflected to the $-x$ direction by ~36° and also exhibits a good directivity (D ~4.7).

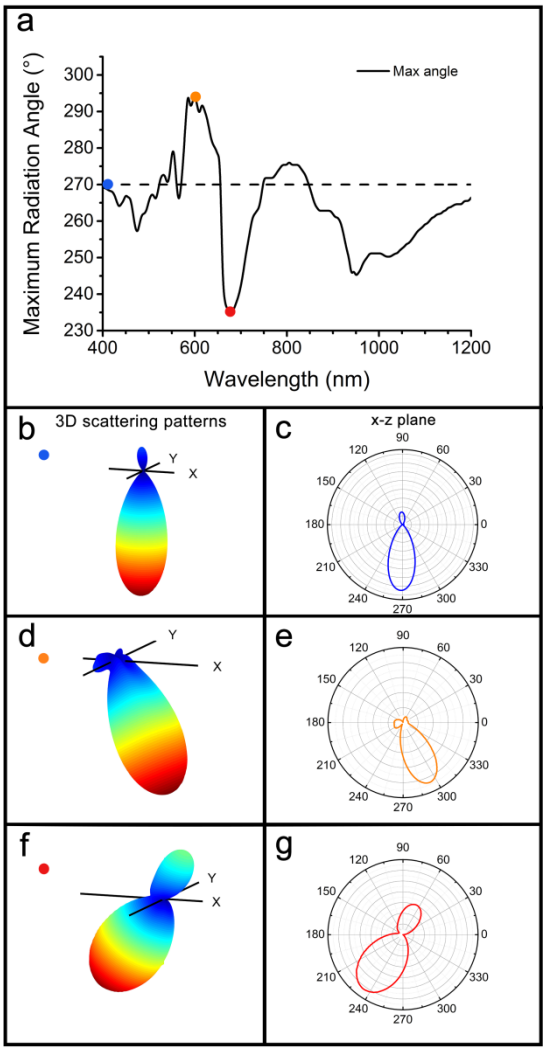

Fig. 9. (a) Wavelength dependence of the maximum radiation angle simulated for the nano-antenna. The 3D radiation patterns calculated at wavelengths of 405, 600, 680 nm are shown in (b), (d), (f) while the corresponding 2D radiation patterns are shown in (c), (e), (g).

In Fig. 9(a), it is noticed that there are two dips appearing at 540 and 565 nm in the wavelength dependence of the maximum radiation angle. They are caused by the F-P mode of the Si cuboids, which deteriorates the radiation direction of the nano-antenna (see Section A2, Appendix).

The simulation results described above were obtained for the nano-antenna suspended in air. The influence of the substrate was not taken into account. In practice, a quartz substrate is generally used as the mechanical support for the nano-antenna. We also performed numerical simulations for the nano-antenna in the presence of a quartz substrate and found that the influence of the quartz substrate with a low refractive index (~1.45) on the performance of the nano-antenna is negligible (see Section A3, Appendix).

Optics EXPRESS

3.5 All-silicon-based nano-antenna for polarization multiplexing

For the simulation results discussed above, the polarization of the incident light is along the *x* direction. In this case, the nano-antenna appears to be asymmetric with respect to the electric field of the incident light. Consequently, an ED component (ED_z) is induced which can be employed to manipulate the radiation direction of the nano-antenna.

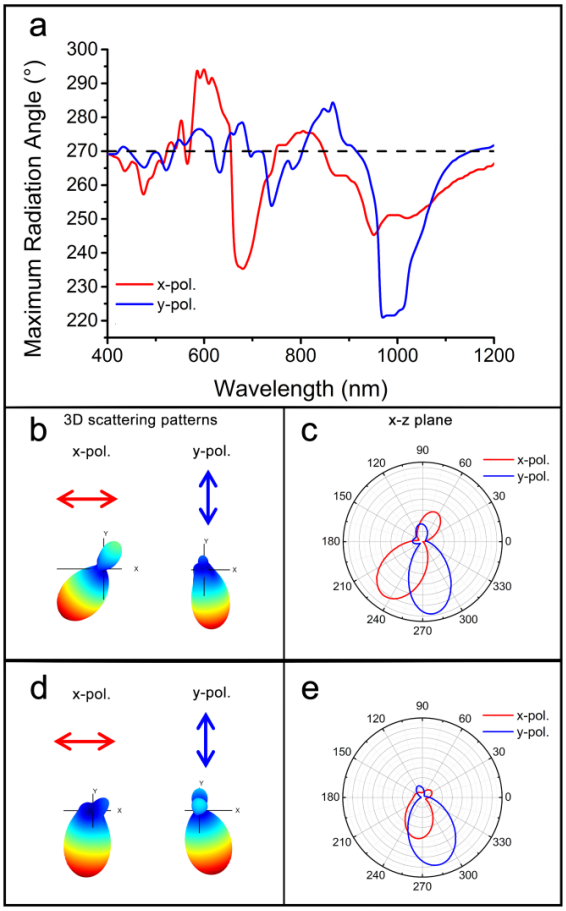

Fig. 10. (a) Wavelength dependence of the maximum radiation angle of the nano-antenna calculated for the incident light whose polarizations are along the x and y directions. (b) and (d) show the 3D radiation patterns calculated at wavelengths of 680 and 860 nm for the x- and y-polarized light. The corresponding 2D radiation patterns are shown in (c) and (e).

If we change the polarization of the incident light to the y direction, then the nano-antenna appears to be asymmetric with respect to the magnetic field of the incident light. Similarly, a MD component (MD_z) is induced and it can be used to control the radiation direction of the nano-antenna.

In Fig. 10(a), we show the wavelength dependence of the maximum radiation angle calculated for the incident light whose polarizations are along the x and y directions. In the long-wavelength regions of [655 nm, 700 nm], [750 nm, 800 nm], and [850 nm, 915 nm], it can be seen that the radiation of the nano-antenna is deflected to different directions (+ x or – x directions), depending strongly on the polarization of the incident light. This feature implies that the nano-antenna functions as a polarization demultiplexer in these wavelength regions, as schematically shown in Fig. 1(b).

Optics EXPRESS

3.6 All-silicon-based nano-antenna array for light bending

We have demonstrated numerically that a single nano-antenna functions as not only a wavelength demultiplexer but also a polarization one. In practice, a device capable of steering light beams with large diameters is highly desirable. We show here that this function can be realized by using an array of nano-antennas. Since the nano-antenna proposed in this work possesses adjustable radiation direction and good directivity, it can be used to construct such an array.

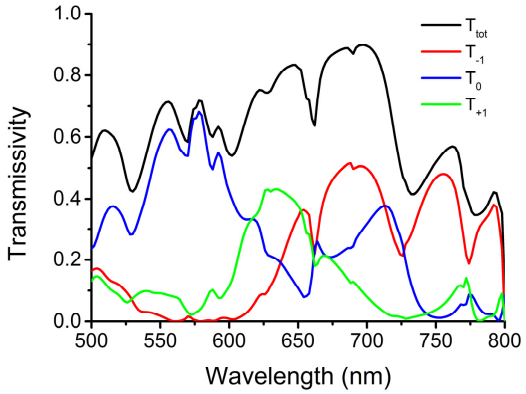

Fig. 11. Transmission spectra calculated for the nano-antenna array whose periods in the x and y directions are designed to be 800 and 450 nm, respectively. T_{tot} is the total transmission while T_{-1}, T_0, and T_{+1} represent the transmissions of the orders of −1, 0, and + 1, respectively.

The device is composed of nano-antennas regularly arranged on a rectangle lattice with a period of d_x = 800 nm in the *x* direction and a period of d_y = 450 nm in the *y* direction. The transmission spectrum simulated for the nano-antenna array is shown in Fig. 11. It can be decomposed into the transmissions of different orders of −1, 0, and 1 (i.e., T_{-1}, T_0, and T_{+1}). In the spectra of T_{+1} and T_{-1}, one can see transmission peaks located at ~630 and 690 nm, which arise from the radiations of single nano-antennas [53,54]. In addition, it can be seen that T_{+1} is larger than T_{-1} in the wavelength region of [530 nm, 650 nm]. However, T_{-1} becomes larger than T_{+1} in the wavelength region [660 nm, 800 nm]. In addition, the wavelength dependence of T_{+1} and T_{-1} is quite similar to the wavelength dependence of the maximum radiation angle (or the deflection angle) of the single nano-antenna.

In Figs. 12(a) and 12(b), we show the 2D electric field distributions of the nano-antenna array on the *xz* plane calculated at wavelengths of 583 and 730 nm. The *x*-polarized light is incident on the quartz substrate. The light normally incident on the substrate is deflected to the left side (-*x* direction) at 583 nm and to the right side (+ *x* direction) at 730 nm. The deflection angles are estimated to be 47° and 63°.

Optics EXPRESS

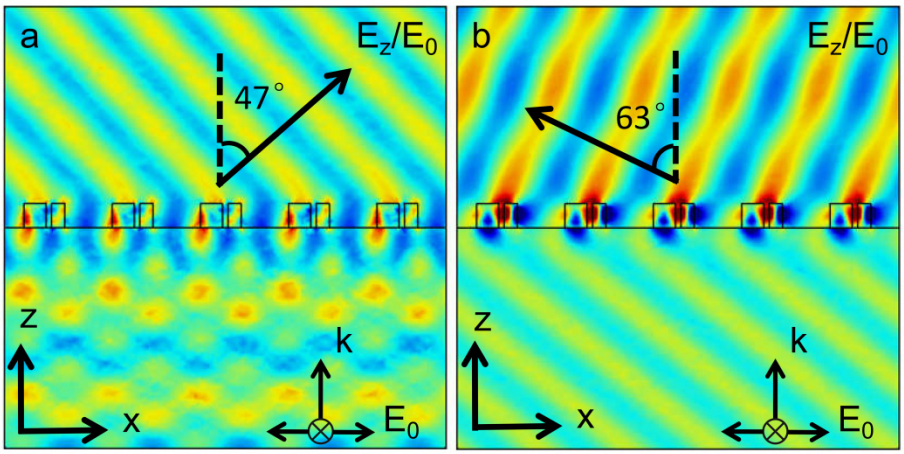

Fig. 12. 2D electric field distribution of the nano-antenna on the xz plane calculated at wavelengths of (a) 583 nm and (b) 730 nm.

4. Conclusion

In summary, we propose an all-silicon-based nano-antenna which is composed of two Si cuboids with the same length and height but different widths. The asymmetric structure of the nano-antenna with respective to the electric/magnetic field of the incident light induces an ED/MD component in the propagation direction of the incident light. The interference of such an ED/MD with the other MD/ED components of the can be employed to manipulate the radiation direction of the nano-antenna. In addition, the interference between the dipoles and the quadrupoles of the nano-antenna can be exploited to shape the radiation directivity of the nano-antenna. It is revealed that the phase difference between the electromagnetic modes plays a crucial role in the interference between them, determining the radiation angle of the nano-antenna. By exploiting the wavelength and polarization dependence of the deflection angle, we demonstrated numerically that the nano-antenna functions as not only a wavelength demultiplexer but also a polarization one. More interestingly, we show that a nano-antenna array composed of regularly arranged nano-antennas can be employed to steer the propagation direction of light beams with large diameters when the diffractions of the array are intentionally designed to be coincide with the deflection angles of single nano-antennas. For practical applications, the all-silicon nano-antennas sitting on a quartz substrate can be experimentally fabricated by using the techniques of wafer bonding, electron-beam lithography and reactive ion etching [55]. Apart from the wavelength and polarization demultiplexers proposed in this work, such nano-antennas may find possible applications in single photon emitters.

Appendix

A1 KK conditions in germanium and silicon nanospheres

The first and second Kerker's conditions for Ge and Si nanoparticles have been discussed in [28] and [56]. Here, we examined Ge and Si nanospheres (NSs) with the same diameter of 75 nm. The multipole expansion of the total scattering for the Ge and Si NSs are shown in Fig. 13(a) and Fig. 13(b). The wavelengths at which the first and second Kerker's conditions are indicated by green and blue points. In addition, the wavelengths at which the largest ratios of the forward to backward scattering and the backward to forward scattering are indicated by red and orange points. In Fig. 13(c) and Fig. 13(d), we show the wavelength dependence of the phase difference between the electric dipole and the magnetic dipole induced in the Ge and Si NSs, respectively. It can be seen that the largest ratios of the forward to backward

Optics EXPRESS

scattering and the backward to forward scattering are not achieved at the wavelength where the amplitudes of the ED and MD are equal. Instead, they are obtained at the wavelength where the ED and MD have the similar amplitudes and a phase difference close to 0 or π.

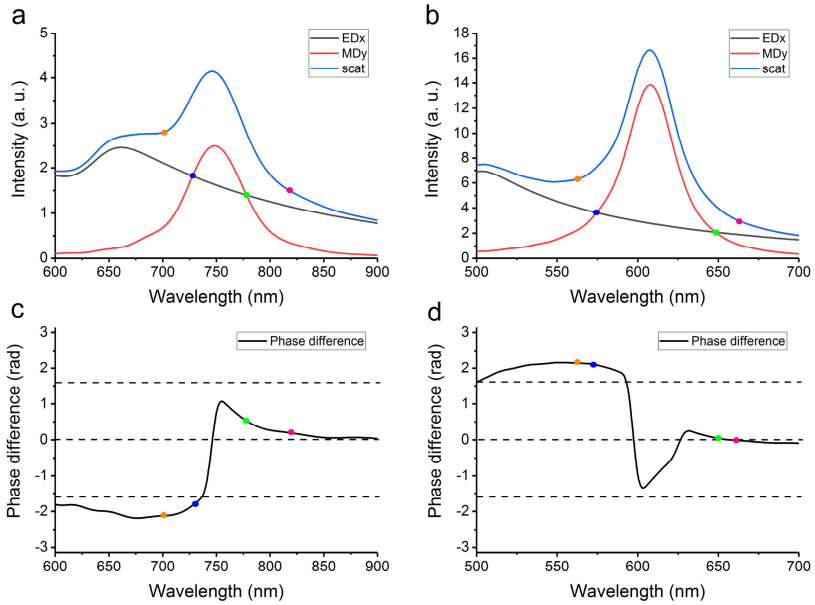

Fig. 13. Multipole expansion of the total scattering spectrum calculated for a Ge (a) and a Si (b) nanosphere with a diameter of 75 nm. The wavelength dependence of the phase difference between the Ed and MD induced in the Ge and Si NSs are shown in (c) and (d), respectively.

A2 Fabri-Perot mode in Si cuboids

The F-P mode intrinsically induced in Si cuboids will deteriorate the radiation directivity of the nano-antenna. In Figs. 14(a) and 14(b), we show the electric field distributions calculated for the small and large Si cuboids of the nano-antenna at 541 nm and 565 nm. The influence of the F-P mode on the radiation properties of the nano-antenna can be found in previous literature [57].

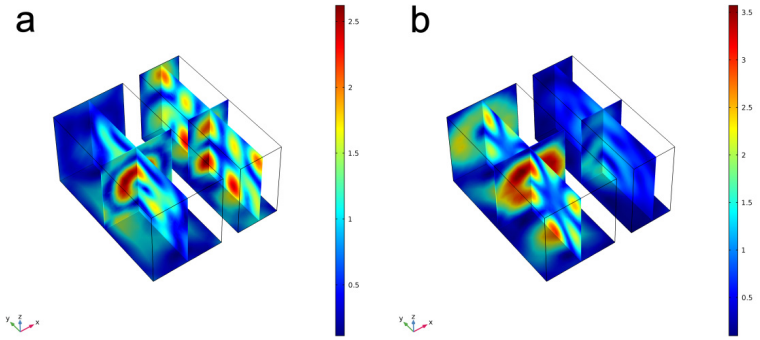

Fig. 14. Electric field distributions calculated for the small (a) and large (b) Si cuboids of the nano-antenna at 541 and 565 nm, respectively.

A3 Radiation of the nano-antenna on a glass substrate

In Fig. 15, we show the 3D and 2D radiation patterns calculated for a nano-antenna placed on a quartz substrate. The simulation method is similar to that described in [37]. The refractive

Optics EXPRESS

index of the quartz substrate was chosen to be 1.45. The largest deflection angles to the +x and -x directions are achieved at 615 and 680 nm, which are quite similar to those observed for the nano-antenna suspended in air. It implies that the influence of the substrate with a low refractive index on the radiation properties of the nano-antenna is negligible.

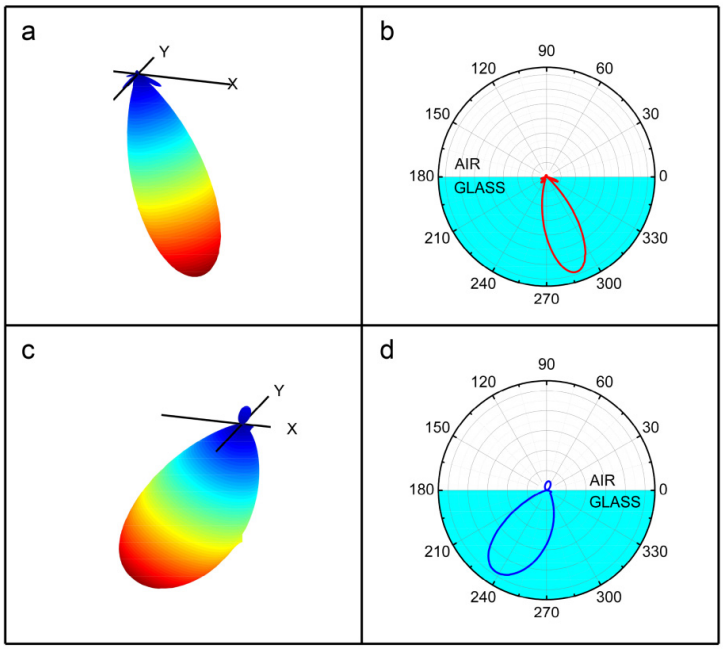

Fig. 15. (a) Radiation patterns calculated for the nano-antenna placed on a quartz substrate with a refractive index of 1.45 at (a) 615 nm and (b) 680 nm. The deflection angles achieved at these two wavelengths are + 18.8° and −30.6°.

Funding

National Natural Science Foundation of China (NSFC) (Grant No. 11674110); Natural Science Foundation of Guangdong Province, China (Grant No. 2016A030308010); Science and Technology Planning Project of Guangdong Province, China (Grant No. 2015B090927006); Innovation Project of Graduate School of South China Normal University (Grant No. 2017LKXM089).